Photoelectron Spectromicroscopy of Potassium Redistribution in the $O_2 + H_2$ Reaction on Rh(110)

H. Marbach,[†] S. Günther,[†] T. Neubrand,[†] R. Hoyer,[†] L. Gregoratti,[‡] M. Kiskinova,[‡] and R. Imbihl*,[†]

Institut für Physikalische Chemie und Elektrochemie, Universität Hannover, Callinstrasse 3-3a, D-30167 Hannover, Germany, and Sincrotrone Trieste, Area Science Park-Basovizza, I-34012 Trieste, Italy

Received: March 23, 2004; In Final Form: June 16, 2004

The reversible condensation of potassium into large K + O coadsorption islands that occurs during the $O_2 + H_2$ reaction on a Rh(110) surface predosed with potassium has been studied in the 10^{-7} mbar range at temperatures between 533 and 623 K and with K coverages between 0.025 and 0.11 ML. Scanning photoelectron microscopy has been used as a spatially resolving in situ method to follow the development of the condensation process via calibrated K and O profiles. A Pt patch evaporated onto the Rh(110) surface served as a nucleation center for the reaction fronts. The coadsorbate phases evolving in the course of the condensation were characterized by local photoelectron spectra. Only at high enough temperature (∼580 K) is a nearly complete redistribution of the potassium by reaction fronts observed, whereas at low temperature, a substantial amount of the K + O coadsorbate remains on the reduced surface. The formation of a high-coverage (8 × 2) K + O phase characterized by an energy-shifted component in the Rh 3d and O 1s peaks appears to play a particular role in the condensation process.

1. Introduction

Alkali metals have always played an important role both in fundamentally oriented surface science studies as well as in practical industrial catalysis.[1−4] Their characteristic property is that, at low coverages,, adsorption of the alkali metal is accompanied by an electronic transfer to a transition metal, thus forming an adsorbate complex with a high dipole moment that strongly lowers the work function of the transition metal surface. Alkali metals are highly reactive, and their chemical state can also be described as ionic when they are coadsorbed with electron-acceptor species, such as O, OH, N, CO, etc. This is why it is now believed that the modified catalyst properties are determined exclusively by the changes induced in the electrostatic potential in the vicinity of the alkali adatoms.[5]

Along with high reactivity, another distinct feature of alkali adatoms is that they are highly mobile in absence of coadsorbates, and these properties were shown to induce pattern formation in catalytic reactions. As was demonstrated with the $O_2 + H_2$ reaction on a Rh(110) surface predosed with potassium, the reaction fronts transport potassium.[6−9] A stationary concentration pattern results as a stable final state in which potassium is coadsorbed with oxygen in islands of macroscopic size. This process has been followed in situ with photoemission electron microscopy (PEEM) and scanning photoelectron microscopy (SPEM) as spatially resolving methods.

Initiated by the above-mentioned findings, the phase diagrams of the alkali adsorption system Rh(110)/K as well as of the coadsorption system Rh(110)/K + O were investigated in detail.[10] As could be anticipated from the large variety of different reconstruction phases that already exist for Rh(110)/O, the coadsorption phase diagram is very rich.[11,12] To demonstrate the participation of ordered coadsorbate phases, a low-energy electron microscopy (LEEM) study was carried out, showing that the whole condensation process proceeds, in fact, via ordered overlayers.[9] A photoelectron spectroscopic characterization of the phases in Rh(110)/K as well as in the coadsorption system Rh(110)/K + O has been conducted.[13] This study also showed that the reactivity of oxygen toward H_2 is dramatically reduced in the presence of coadsorbed potassium. Mathematical modeling based on experimental data could reproduce nearly all of the essential experimental facts of the condensation process.[7,14]

In this paper, we study the properties of front propagation in this system in detail, focusing on the differences from a simple bistable system where a front moves with constant profile and velocity. Such behavior is clearly not observed here. A second goal is to conduct an in situ spectroscopic characterization of the condensed phase that finally forms to understand the driving force for the condensation process. Using calibrated K concentration profiles, we obtain a more quantitative characterization of the system, allowing us to correlate the SPEM measurements with the Rh(110)/K + O phase diagram and to establish a database for quantitative modeling.

2. Experimental Section

2.1. Experimental Setup and Sample Preparation. All experiments were carried out in two ultrahigh vacuum (UHV) chambers operated as continuous-flow reactors. The SPEM measurements and part of the PEEM studies were conducted at the electron storage ring ELETTRA. Both systems were equipped to conduct Auger electron spectroscopy (AES), quadrupole mass spectrometry (QMS), and low-energy electron diffraction (LEED).

* To whom correspondence should be addressed. E-mail: imbihl@pci.uni-hannover.de.
[†] Universität Hannover.
[‡] Sincrotrone Trieste.

10.1021/jp048721y CCC: $27.50
Published on Web 08/28/2004

The SPEM measurements were performed at the ESCA microscopy beamline of ELETTRA using photons with an energy of 641 eV. In SPEM, the X-ray beam from the synchrotron light source is focused into a small spot of ~0.15-μm diameter by means of zone plate optics.[15] The microscope works in two modes: imaging and local spectroscopy. By tuning the hemispherical analyzer (HA) to the core-level energy of a certain element and scanning the sample, one obtains a two-dimensional map of the elemental distribution. In the local spectroscopy mode, the energy resolution of the SPEM was ~0.40 eV for Rh 3d and ~0.75 eV for O 1s. In PEEM, the sample is illuminated with photons from a deuterium discharge UV lamp (5.2−6 eV). Because the number of emitted photoelectrons depends on the work function PEEM images primarily the local work function of the sample.

The Rh(110) surface was cleaned by repeated cycles of Ar ion sputtering, oxygen treatments, and annealing to 1200 K. The cleanness of the sample was judged by means of XPS and by the appearance of the various oxygen-induced surface reconstructions in the LEED data during exposure to O_2.[12] The sample was heated by radiation or by electron bombardment from a tungsten filament. In the SPEM measurements, the temperature could only be determined indirectly by the electric current that was flowing through the filament and that had been calibrated before with a pyrometer.

A circular Pt domain of 125-μm diameter and an estimated thickness of 5 nm was prepared on the Rh(110) surface in UHV via Pt deposition through a mask. Potassium was deposited with commercially available SAES getters. Gases of the highest commercially available purity were used (O_2 5.6, H_2 5.3). All pressures given here have been corrected.

2.2. Calibration of the SPEM and XPS Data. To avoid recalibrations that arise because of the necessary adjustment of the focusing X-ray optics and the electron analyzer after each run, not the absolute counting rates but the ratio of the peak areas of the K 2p and the Rh 3d level, A_K/A_{Rh}, was used for the calibration of the potassium coverage. The following relation takes into account the screening of the Rh 3d signal due to adsorbed potassium and oxygen

$$A_K/A_{Rh} = f(\Theta_K) = (\Theta_K k_K)/(A_{Rh} - \Theta_O l_O - \Theta_K l_K)$$

where k_K is the proportionality constant relating the K 2p intensity, A_K, to the K coverage and l_O and l_K are the proportionality constants describing the weakening of the Rh 3d signal, A_{Rh}, due to adsorbed oxygen and potassium. By introducing samples with well-defined oxygen and potassium coverages, reference spectra were obtained that allowed for the fitting of the measured curve in terms of the proportionality constants. Figure 1 shows the reference points as well as the fitted function. By acquiring sets of (Rh 3d, K 2p, and O 1s) and SPEM images/profiles of the same surface area, the SPEM profiles can be calibrated by taking local photoelectron spectra of Rh 3d and K 2p. The oxygen profiles are calibrated similarly.

Concentration profiles of reaction fronts were taken perpendicular to the front direction with about a 2-s acquisition time per line scan. To reduce the noise level, 10−20 line scans were typically averaged in which the positions of the front relative to each other were corrected by the known propagation velocity of the front.

3. Results

3.1. Front Propagation in the Presence of Potassium. Without potassium, the $O_2 + H_2$ reaction on Rh(110) exhibits simple bistable behavior, with reaction fronts initiating transitions between an inactive oxygen-covered state of the surface and an active nearly adsorbate-free state of the surface.[16,17] With coadsorbed potassium, reaction fronts still exist, but they now transport potassium. The starting point is that of a homogeneously oxygen- and potassium-covered surface held in an O_2 atmosphere. When we now increase p_{H_2} to the point when a reduction front is ignited, we observe an adsorbate distribution as displayed in the 2D SPEM images in Figure 2. The circular spot seen in the center of the images is a Pt patch evaporated onto the Rh(110) surface, which serves no purpose other than to act as an easily detectable nucleation center in the SPEM measurements. The reduction front nucleates at the boundary of the Pt patch and then spreads outward, reactively removing chemisorbed oxygen as demonstrated by the O 1s image in Figure 2. The comparison with the corresponding potassium image reveals not only that oxygen is removed but also that potassium is redistributed from the oxygen freed part of the surface to the still oxygen-covered part.[6] The observation that the front positions of oxygen and potassium in the two images do not coincide is simply due to the fact that the images were

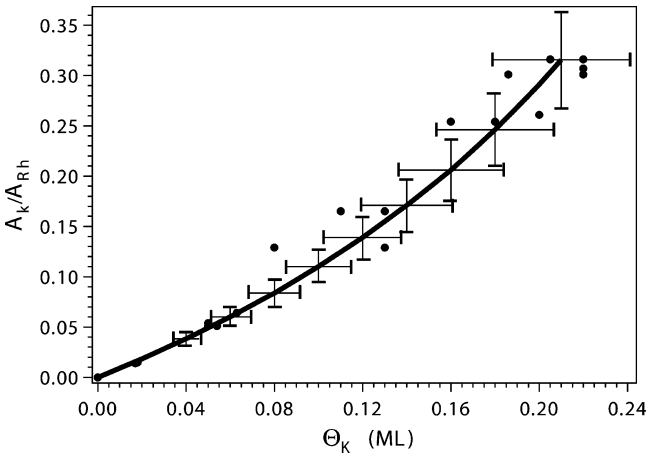

Figure 1. Calibration of the measured ratio of XPS peaks, A_K/A_{Rh}, to the potassium coverage. A_K refers to the area of the K 2p peaks at 291−297 eV, A_{Rh} to the area of the Rh 3d peaks at 305.5−308.5 eV. The data have been fitted to a functional dependence (see text).

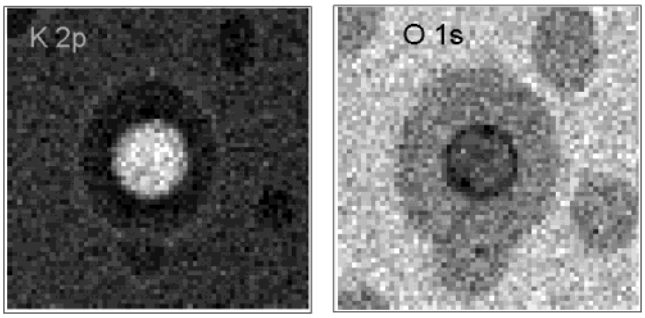

Figure 2. Propagation of reduction fronts during the $O_2 + H_2$ reaction on an oxygen-covered Rh(110) surface predosed with potassium. K 2p and O 1s images (256 × 256 μm^2) taken 17 and 23 min after 'ignition'. In these images a brighter gray level reflects a higher count rate, i.e., a higher concentration. The central bright feature in the K2p image and the central dark spot in the O1s image reflect a Pt patch of 70 μm diameter on the perimeter of which the front nucleated. The position of the front is 30 μm further outward in the K 2p image and 40 μm further outward in the O 1s image. Experimental conditions: $T \approx 550$ K, $p_{O_2} = 3.9 \times 10^{-7}$ mbar, $p_{H_2} = 1.7 \times 10^{-7}$ mbar. Acquisition times of the 2D scans are 2100 s for the O 1s image and 1500 s for the K 2p image.

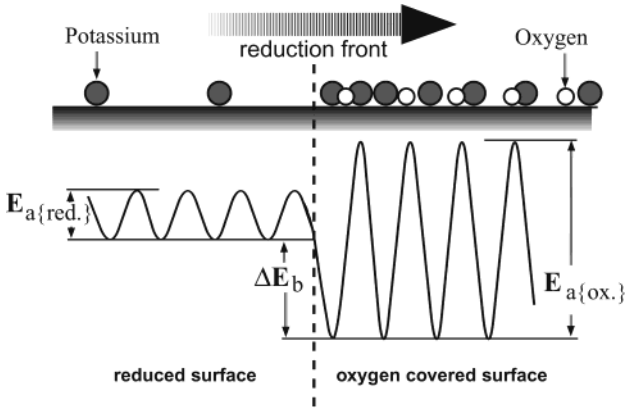

Figure 3. Schematic potential energy diagram for potassium atoms at the interface of the "reduced"/oxygen-covered surface. The energy corrugation reflects the periodicity of the surface. The gain in adsorption energy in the coadsorbed state is denoted as ΔE_b; the differently high activation barriers for diffusion on the oxygen-covered and the reduced surface are represented as $E_{a(ox)}$ and $E_{a(red)}$, respectively.

taken at different time moments. In general, the positions of the potassium and oxygen fronts practically coincide.

The high chemical affinity of oxygen and potassium is clearly the driving force for mass transport toward the O-covered surface. The thermodynamic driving force for the condensation process can best be visualized with the energy diagram in Figure 3, showing the energy profile for a potassium atom moving on a partially reduced Rh(110) surface. The reduction front divides the surface into two halves, with the left half being oxygen-free while the right half is still oxygen-covered. Well supported by simulations with a realistic model, the following key elements for the transport process can be given:[7,14] (1) a gain in adsorption energy as potassium atoms move from the reduced part to the still oxygen-covered part denoted as ΔE_b in the diagram and (2) a change in the potassium mobility on the oxygen-covered and reduced part, i.e., potassium diffuses rapidly on the reduced surface and rather slowly on the oxygen-covered surface. This is denoted in Figure 3 via activation barriers of different heights for K diffusion.

The gain in adsorption energy for coadsorbed potassium shows up in thermal desorption spectroscopy as a shift of the K desorption peak by up to 80 K toward higher temperature. The diffusion process of potassium on the oxygen-covered/reduced surface has been followed in the homogenization process that is initiated after condensation by turning off one of the supply gases.[8] It has been demonstrated earlier that mass conservation of potassium is fulfilled to within 5%, which means that potassium is mainly redistributed on the surface during the condensation process.[6] In the temperature range investigated here, the desorption of potassium presumably plays no role.

In the following discussion, we examine the process depicted already in the 2D SPEM images in Figure 2 using calibrated 1D K concentration profiles. Starting from a homogeneously oxygen- and potassium-covered surface in an $O_2 + H_2$ atmosphere with $\Theta_K \approx 0.1$ ML and $\Theta_O \approx 0.73$ ML, p_{H_2} was increased to the point where a reduction front was initiated at the Pt patch. Figure 4 displays the K coverage profiles from the point of the nucleation of the front until the formation of a stable K + O coadsorption island. This condensed phase develops as the reaction fronts with increasing K redistribution become slower and slower, until finally a stationary pattern consisting of the K + O coadsorption islands develops.

As already outlined in ref 6, pattern formation in this system is anisotropic, and most of the large condensation islands are strongly elongated in the [001]-direction. The [1$\bar{1}$0] direction, along which the concentration profiles shown here were taken, is the direction perpendicular to the reaction front.

The K concentration profiles show that the reduced part of the surface has lost about 80% of the initial K coverage. In the front region, a strong K enrichment is seen, and on the still oxygen-covered part ahead of the front, the K coverage increases with the progression of the front. During this process, the initially sharp K peak at the front position broadens progressively while simultaneously growing in height (Figure 4a−d). From profile d to profile e in Figure 4, the maximum coverage seems to saturate at $\Theta_K \approx 0.16$. A second strong rise of the K coverage to $\Theta_K \approx 0.20$ occurs when a second front moving in opposite direction enters the imaged region so that the potassium is squeezed between the two fronts. Finally, after ~2000 s, a stationary state, represented by profile f in Figure 4, is reached that is characterized by zero front velocity and high coverages of oxygen and potassium, i.e., $\Theta_K \approx 0.20$ and $\Theta_O \approx 0.9$.

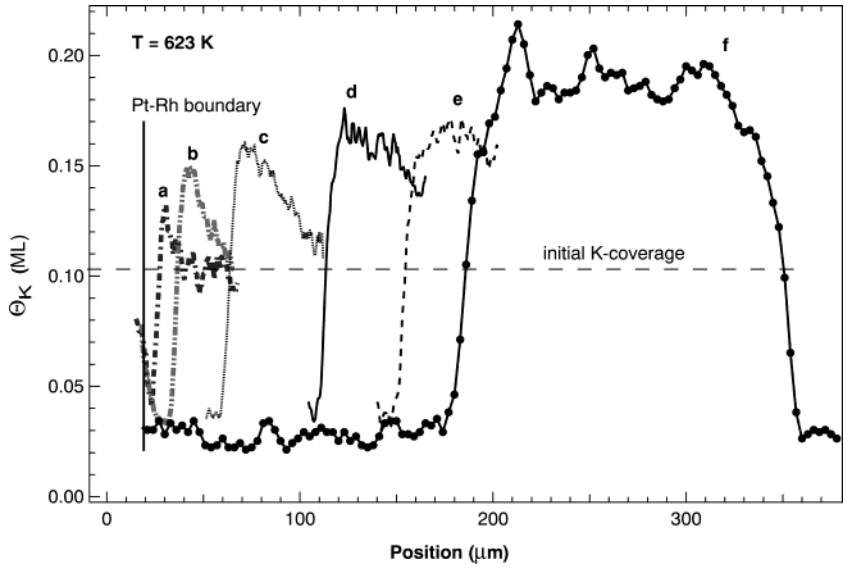

Figure 4. K concentration profiles in the [1$\bar{1}$0] direction demonstrating various stages in the condensation process of the K + O coadsorbate during the reaction at $T = 623$ K. With $t = 0$ denoting the ignition time, profiles were recorded at (a) 10, (b) 117, (c) 364, (d) 1039, (e) 1769, and (f) 2929 s. Experimental conditions: $\theta_K = 0.08$, $T \approx 623$ K, $p_{O_2} = 1.3 \times 10^{-7}$ mbar, $p_{H_2} = 1.32 \times 10^{-7}$ mbar.

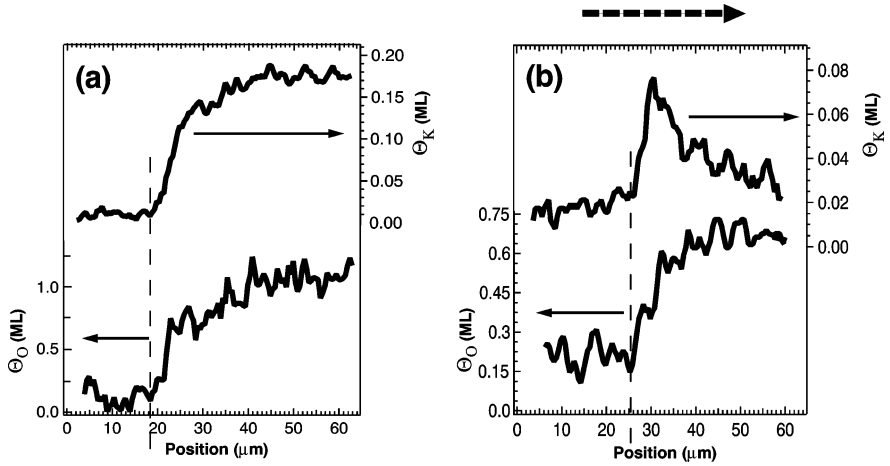

Figure 5. K and O concentration profiles demonstrating the correlation between the two adsorbate coverages in (a) a stationary concentration pattern and (b) a propagating reduction front. The large arrow at the top of b denotes the direction of front propagation. Experimental conditions: (a) $\theta_K = 0.08$, $T \approx 583$ K, $p_{O_2} = 1.3 \times 10^{-7}$ mbar, $p_{H_2} = 0.76 \times 10^{-7}$ mbar; (b) $\theta_K = 0.025$, $T \approx 563$ K, $p_{O_2} = 1.3 \times 10^{-7}$ mbar, $p_{H_2} = 1.09 \times 10^{-7}$ mbar.

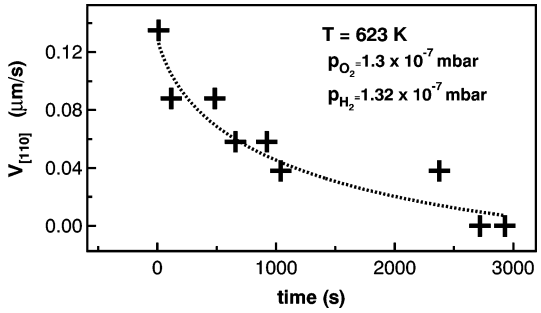

Figure 6. Development of the front velocity with time during the condensation process at $T = 623$ K as depicted in Figure 4. Experimental conditions: $\theta_K = 0.08$, $p_{O_2} = 1.3 \times 10^{-7}$ mbar, $p_{H_2} = 1.32 \times 10^{-7}$ mbar.

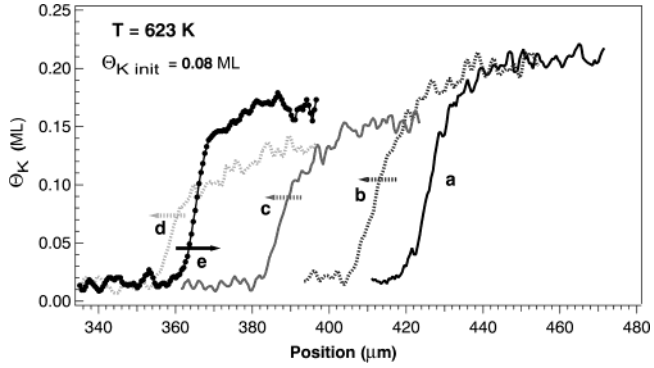

Figure 7. K profiles demonstrating the reversal of front propagation by a parameter change. (a) A reduction front propagating from left right was stopped by decreasing p_{H_2}. (b−d) Further decrease of p_{H_2} to 0.66×10^{-7} mbar caused the front to move in the opposite direction. (e) A second reversal of the direction of front propagation was initiated by increasing p_{H_2} to 0.75×10^{-7} mbar. Experimental conditions: (a) $\theta_K = 0.08$, $T \approx 623$ K, $p_{O_2} = 1.3 \times 10^{-7}$ mbar. Prior to a, p_{H_2} was varied in a range $(0.85-1.5) \times 10^{-7}$ mbar.

The oxygen and potassium profiles cannot be measured simultaneously with SPEM, but by rapidly switching the analyzer energy during rastering, a reliable correlation can be established. The correlation between the potassium profile and the corresponding oxygen profile is depicted in Figure 5 for the cases of (a) a stationary concentration pattern and (b) a propagating reduction front. In contrast to the K profile, the "steplike" oxygen profile in the front region does not change significantly during progression of the reaction front. Only in the final stage of the condensation process does the oxygen coverage increase significantly, reaching a higher level of $\Theta_O \approx 1.0-1.1$ at $\Theta_K \approx 0.18$ compared to the $\Theta_O \approx 0.7$ for the propagating front.

In contrast to a bistable system, both the front profile and the front velocity are not constant but change continuously. The decrease of the front velocity along the $[1\bar{1}0]$ direction is reproduced in Figure 6. The front velocity decreases initially very steeply from 0.13 μm/s to about half of this value within 500 s, followed by a very smooth decay over the next hour.

In a bistable system, the direction of front propagation can be reversed by a corresponding parameter change, and only for one particular parameter, the equistability point, is the front velocity zero, i.e., both phases are equally stable.[18] Attempts to induce a reversal of front propagation by a p_{H_2} decrease were not successful at $T < 570$ K, and it was therefore first believed that this is a general property of this system. At higher temperature, however, such a reversal can be achieved, as demonstrated by the K concentration profiles in Figure 7 taken at $T = 623$ K. Starting from a situation close to a stationary condensation phase shown by profile a, a front reversal was initiated by reducing p_{H_2} from 0.87×10^{-7} to 0.66×10^{-7} mbar. This decrease caused the reduction front that was still advancing slowly first to stop and then to retract, thus becoming an oxidation front. Profiles b−d in Figure 7 demonstrate that, first, the K enrichment in the front region is absent and, second, the potassium coverage in the K + O coadsorbate phase strongly decreases. Increasing p_{H_2} to 0.76×10^{-7} mbar causes the front once more to reverse its propagation direction associated with a pronounced increase of the K concentration in the K + O region, as indicated by profile e. A decrease of the K concentration inside the K + O island with expanding boundaries naturally follows from mass conservation. More surprising might be the absence of a K enrichment in the front region, but as is demonstrated below, the enrichment is actually a kinetic phenomenon bound to a certain distribution of potassium that has to be far from the equilibrium distribution.[7]

The enrichment of potassium in the front region can be explained as a kinetic effect using the energy diagram of Figure 3.[7,14] As K atoms, which are very mobile on the reduced part of the surface invade the oxygen-covered part of the surface, they are slowed strongly as a consequence of the higher activation energy for surface diffusion indicated in Figure 3. Because redistribution of potassium is slow on the oxygen-

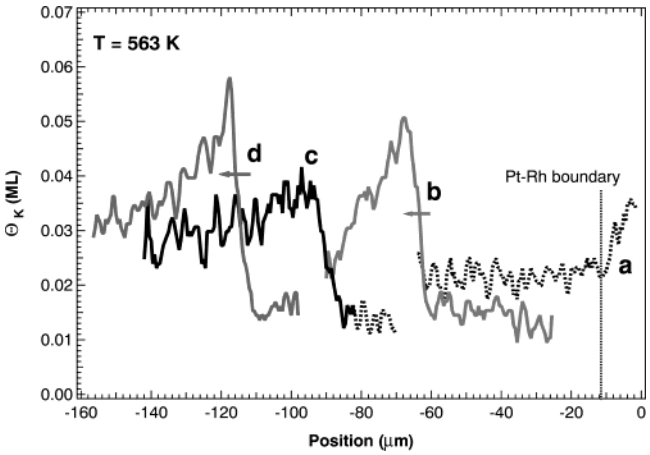

Figure 8. Experiment demonstrating that the enrichment of potassium in the front region is due to kinetics. Starting from a homogeneous K distribution on a O-covered surface (a, $t = 0$ s), a reduction front was initiated at the Pt/Rh interface. The propagating front (b, $t = 369$ s) was stopped by decreasing p_{H_2} to 0.66×10^{-7} mbar (c, $t = 815$ s). Increasing p_{H_2} to 1.09×10^{-7} mbar caused the front to propagate again (d, $t = 1004$ s). Experimental conditions: $\theta_K = 0.08$, $T \approx 563$ K, $p_{O_2} = 1.3 \times 10^{-7}$ mbar.

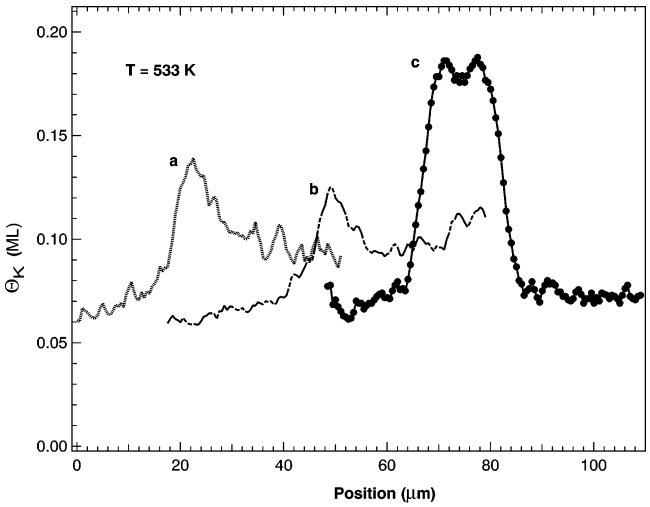

Figure 9. K concentration profiles in the [110] direction demonstrating an incomplete redistribution of potassium in the condensation process at lower temperature, i.e., $T = 533$ K. With $t = 0$ denoting the start of the experiment, profiles were recorded at (a) 2288, (b) 2448, and (c) 2948 s. Experimental conditions: $\theta_K = 0.08$, $p_{O_2} = 1.3 \times 10^{-7}$ mbar, p_{H_2} = (a,b) 1.75×10^{-7} mbar, (c) 1.65×10^{-7} mbar.

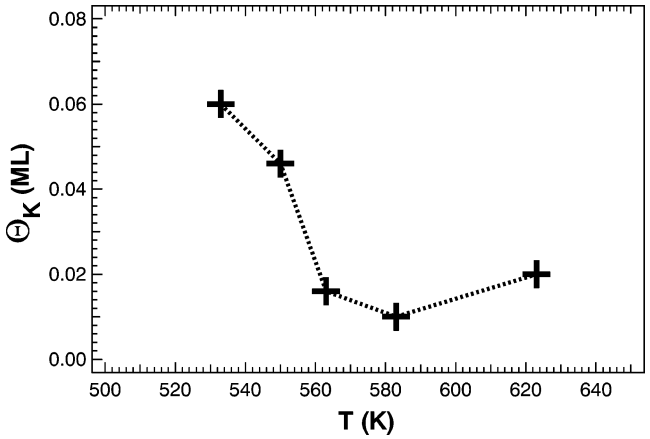

Figure 10. Remaining potassium coverage on the reduced part of the surface vs temperature. Experimental conditions: $\theta_K = 0.08$, $p_{O_2} = 1.3 \times 10^{-7}$ mbar, p_{H_2} varied.

covered part, a high concentration builds up in the interface region. This interpretation is bolstered by numerical simulations but alternatively, one might also think of a thermodynamic stabilization given by a different chemical environment in the front region. For example, one might have a substantial OH coverage in the front region keeping the potassium bound there.

To answer this question, the following experiment displayed in Figure 8 was performed. After initiation of a reduction front (a,b), this front was stopped by a p_{H_2} decrease (c). As demonstrated by the corresponding K concentration profiles in Figure 8, the halting of the front causes a flattening of the K profile in the front region. Restarting the reduction front (d) by a p_{H_2} increase leads back to the strong K enrichment in the front region. If the enhanced K concentration in the front region were caused by thermodynamic stabilization—for example, by a high OH coverage—then the front profile should not change when the front is stopped. The observed change in the K concentration profile fully supports the kinetic mechanism. According to this mechanism, a moving front is required to obtain K enrichment in the front region. Stopping the front allows the high K coverage in the front region enough time to spread out diffusively on the oxygen-covered part of the surface so that the profile becomes flat.

SPEM measurements of front propagation in the system Rh(110)/K/O_2 + H_2 were carried out at a total of five different temperatures, namely, 533, 551, 563, 583, and 623 K. The K concentration profiles at 533 K, which is nearly 100 K lower than the temperature used in the previous experiments, are displayed in Figure 9. In contrast to the development at 623 K, a relatively high K coverage of 0.06−0.07 remains on the reduced surface. Apparently, only at a high enough temperature does a nearly complete redistribution of the potassium from the reduced into the oxygen-covered part take place, whereas at low temperature, a substantial K coverage remains on the reduced part of the surface. Oxygen O 1s spectra demonstrate that, at low temperature, the surface is only partially reduced, and the remaining oxygen coverage of 0.46 measured for $T = 533$ K apparently stabilizes the potassium.

A plot of the K coverage on the reduced surface versus the temperature is displayed in Figure 10. The residual K coverage on the reduced surface decreases strongly from 0.06 to 0.01 at 583 K. At higher temperature, $T = 623$ K, an increase to 0.02 is seen that probably results from the backflow of potassium when the K-saturation coverage is exceeded in the K + O phase. In the condensed phase, the K coverage at $T = 533$ K reaches only 0.18 (Figure 9, curve c), which is much lower than the 0.24 ML obtained at 623 K.

3.2. Spectroscopic Characterization of the Condensed Phase. For characterization of the different phases and the bonding states of the adsorbates, the main tool is photoelectron spectroscopy. The large K + O island depicted in profile f of Figure 4 is stationary for the given reaction conditions, but when we increase p_{H_2}, we observe a further compression of the islands leading to a correspondingly higher K coverage inside. This condensation island, whose K profile is reproduced in Figure 11a, apparently represents the limiting case in the condensation process because a higher K coverage could not be achieved in any experiment through variation of the parameters.

The K concentration profile reveals two distinct phases: a phase with $\Theta_K \approx 0.24$ in the center, which we denote as the high-coverage condensation phase (HCCP), and a phase with $\Theta_K \approx 0.18$ showing up as shoulder, which we call the low-coverage condensation phase (LCCP). Rh $3d_{5/2}$ spectra repro-

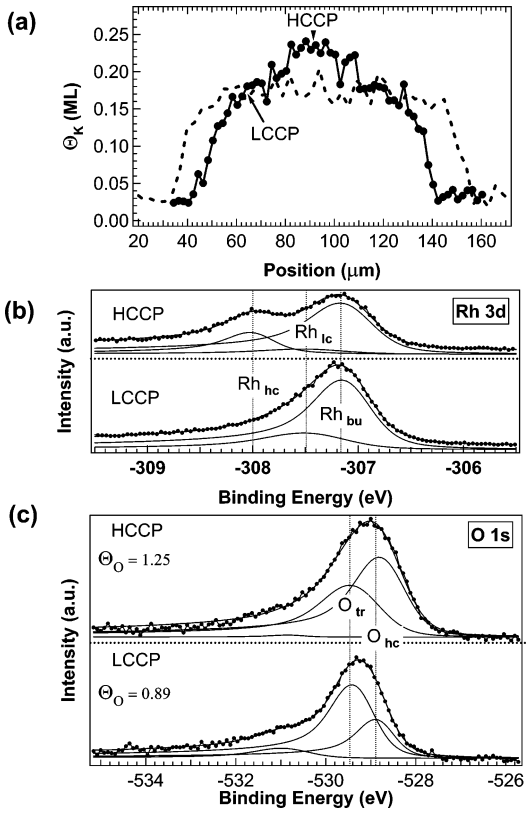

Figure 11. Spectroscopic characterization of the condensed phase at $T = 623$ K in the experiment depicted in Figure 4 by (a) Rh 3d and (c) O 1s photoelectron spectra. The two K profiles in a represent the stationary condensed phase at $p_{H_2} = 1.32 \times 10^{-7}$ mbar (dashed line) and after a p_{H_2} increase to 1.51×10^{-7} mbar caused a further contraction of the phase (filled circles). Local photoelectron spectra of the Rh3 d and O 1s regions in b and c characterize the LCCP and HCCP phases, respectively (see text). The spectra were fitted with Doniach−Sunjic functions which include a a Lorentzian part, a Gaussian part, and an asymmetry factor. Experimental conditions: $\theta_K = 0.08$, $p_{O_2} = 1.3 \times 10^{-7}$ mbar.

duced in Figure 11b reveal pronounced differences between the two phases. The displayed fits were obtained by using a Lorentzian width of 0.24−0.27 eV and an asymmetry ranging from 0.20 to 0.22.

The Rh $3d_{5/2}$ spectra of the LCCP are similar to the spectra observed of an oxygen-saturated K-free Rh surface. It contains the bulk Rh $3d_{5/2}$ component at 307.2 eV and the O-related surface core level component at ∼307.5 eV. An additional component at ∼308.0 eV develops in the HCCP phase. As discussed in our previous study the 308.0 eV component is indicative either of formation of a thin oxide layer or of surface Rh atoms coordinated with four oxygen adatoms.[10,13,19,20] The O 1s spectra displayed in Figure 11c have two main components at ∼529.5 and 528.8 eV. For the displayed O 1s fits, a Lorentzian width of 0.30 eV and an asymmetry of 0.19 were used. The 529.5 eV component corresponds to oxygen sitting in 3-fold sites between the top and second layer along "1 × 2" troughs of the (1 × 2) reconstructed Rh surface,[22] whereas the 528.8 eV is correlated with the 308.0 eV Rh $3d_{5/2}$ component, i.e., it reflects the surface oxide where the O coverage exceeds 1 ML.[10] In fact, the oxygen coverage in the HCCP phase is quite high with $\Theta_O = 1.25$ compared to Rh(110)/O_2, where the maximum oxygen coverage is ∼0.75 ML.

The Rh $3d_{5/2}$ and O 1s spectra are practically identical to those measured on the "segmented" (8 × 2) phase formed in the K + O coadsorption system at $\Theta_K = 0.25$.[13] In this phase, a (1 × 2) "missing-row" reconstruction is present with segmented [1$\bar{1}$0] rows consisting of six Rh atoms on eight substrate sites. Similar segments were seen on the K-free (10 × 2) O surface structure with eight Rh atoms on 10 sites.[21] According to theoretical predictions, this segmented structure should allow the accommodation of four oxygen atoms per Rh atom in the outermost [1$\bar{1}$0] row, leading to an oxygen coverage of up to ∼0.8 ML.[10] On a K-covered surface oxygen can also adsorb onto the (111) microfacets, which is consistent with the experimentally observed higher oxygen coverage. The same (8 × 2) structure was also detected in the condensed phase in a LEEM/μ-LEED study.[9]

The LCCP with $\Theta_K = 0.17$ and $\Theta_O = 0.89$ cannot be as clearly assigned to a coadsorbate structure as was the case with the HCCP. A 528.8 eV component is present in the O 1s spectra and the 308.0 eV component is absent in the Rh 3d peak.

At 533 K, the oxygen species at the 528.8 eV position of the HCCP appears, but in the Rh 3d spectra the corresponding R_{hc} component is missing, similarly to the LCCP spectrum in Figure 11c. We therefore conclude that no HCCP is formed at 533 K. These experiments show that the reaction temperature has a decisive influence on the formation of the HCCP, which develops only at $T > 570$ K, in accordance with the K + O coadsorption studies.[13] At $T < 570$ K, we observed essentially only the spectroscopic features of the low-coverage condensation phase.

The existence of two states of the condensed K + O phase is further supported by a titration experiment at 583 K reproduced by a series of K profiles in Figure 12. In this experiment, the reaction conditions were varied a couple times over a period of several hours to generate defined reference states for the photoelectron spectra. After initiation of a reduction front, this front was stopped by decreasing p_{H_2}. Afterwards, oxidizing conditions were adjusted by turning off the H_2. The K concentration profile in part a of Figure 12 shows the smoothing of the initially steep front profile due to the slow diffusive spreading of potassium on the oxygen-covered surface.

After the oxygen had been turned off, the titration with H_2 ($p_{H_2} = 1.75 \times 10^{-7}$ mbar) was started. Remarkably, shortly after the introduction of H_2, a reaction front was generated as demonstrated by profile b. As in the experiment under stationary conditions, we also observed during H_2 titration that reduction fronts are initiated that redistribute the potassium. The two K profiles b and c of Figure 12 demonstrate how, with the progression of the front, the K concentration level ahead of the front rises to $\Theta_K = 0.19$. The propagation velocity remains constant at about 0.11 ± 0.015 μm/s. A second reduction front coming from the opposite direction squeezes the potassium between the two fronts to a high-coverage K + O condensation island forms as demonstrated by profile d. In contrast to the experiment with stationary reaction conditions, however, the two reduction fronts continue their journey until they collide and annihilate. The potassium originally fenced in by the two fronts then starts to spread out over the surface. This is, of course, what one would expect given that, on a completely reduced surface, a homogeneous distribution of the potassium on the surface should result.[6]

The O 1s and Rh 3d spectra taken at various points of the profile are displayed in Figure 13. The spectra RC were recorded prior to the titration experiment under stationary reaction conditions with both gases, H_2 and O_2, on. The spectra were taken inside the K + O phase from a position about 110 μm away from the reduction front. At this stage of the condensation

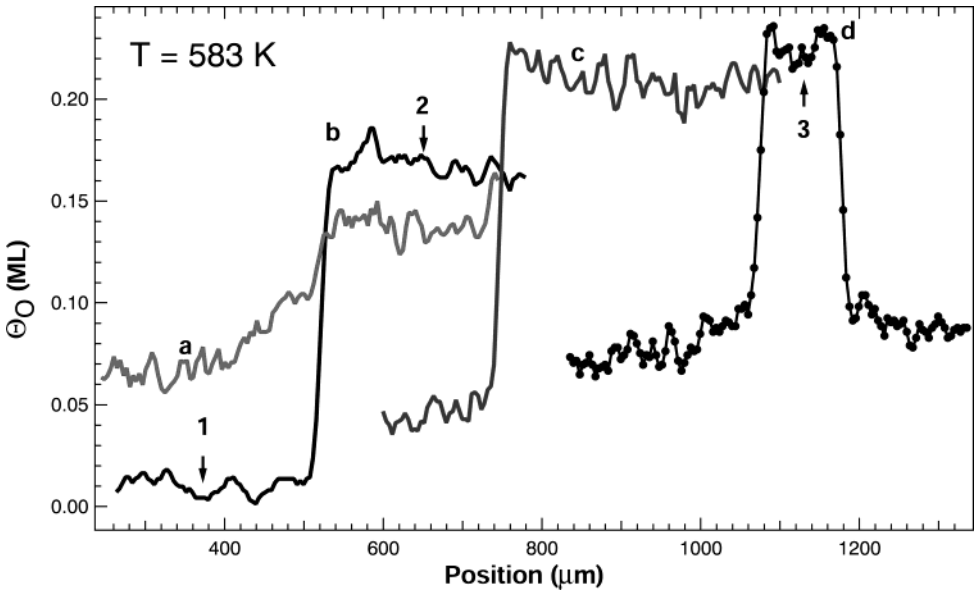

Figure 12. K concentration profiles demonstrating various stages in the condensation process of the K + O coadsorbate during titration of the oxygen-covered surface with H_2 at $T = 583$ K. The various positions at which the coadsorbate structure was characterized by local photoelectron spectra of the Rh 3d and O 1s regions displayed in Figure 11 are indicated. Prior to the experiment displayed here, a reduction front has been initiated in $O_2 + H_2$. (a) Spreading of potassium on the oxygen-covered surface after H_2 has been turned off. (b−d) Progression of reduction fronts during titration with H_2. Experimental conditions: $\theta_K = 0.08$, $p_{O_2} = 1.3 \times 10^{-7}$ mbar, $p_{H_2} = 1.65 \times 10^{-7}$ mbar.

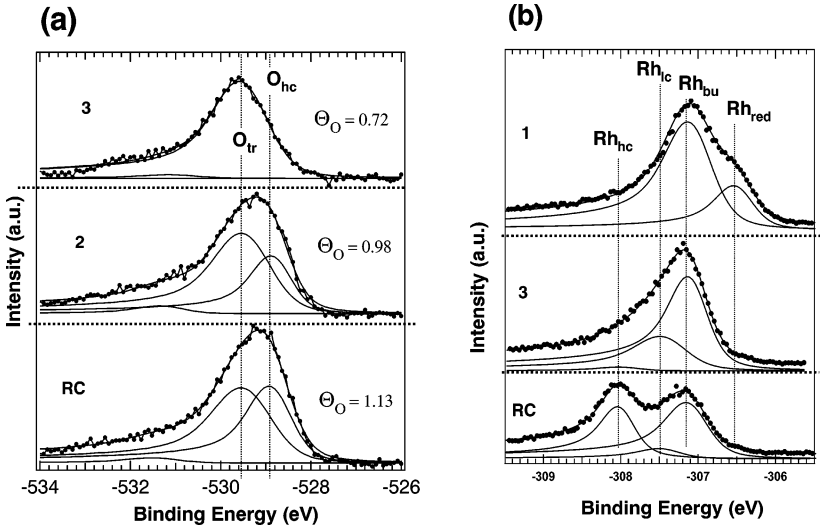

Figure 13. Local (a) O 1s and (b) Rh $3d_{5/2}$ photoelectron spectra demonstrating the removal of different oxygen states during the titration experiment depicted in Figure 10. The numbers 1−3 of the spectra refer to the arrows in Figure 12, RC refers to the K + O coadsorbate phase under stationary reaction conditions. In Figure 13b, Rh_{bu} denotes the bulk component; Rh_{lc} and Rh_{hc} denote the surface components of the LCCP and HCCP, respectively; and Rh_{red} denotes the component of the reduced surface.

process, the HCCP is already present, as evidenced by the O 1s and Rh $3d_{5/2}$ spectra in Figure 13. After the H_2 titration is started, Rh 3d spectrum 1 obtained at position 1 in Figure 12 clearly shows the surface core level peak of the reduced surface. On the oxygen-covered parts of the surface the HCCP-related components are gradually removed as the reduction front progresses (see spectra 2 and 3 corresponding to positions 2 and 3 in Figure 12). When the two reaction fronts finally collide, squeezing in the enclosed potassium to the very high concentration of $\Theta_K = 0.24$, only the O_{tr} component is left, as shown by spectrum 3 in Figure 13. Just from the rather long time that a high oxygen coverage survives in the above titration experiment, decreasing to only $\Theta_O = 0.72$ at $t = 4200$ s after the introduction of H_2, one has to conclude that the reactivity of the K + O phase to hydrogen adsorbing from the gas phase is quite low. Therefore the decrease in oxygen reactivity is most likely due to a strongly reduced hydrogen sticking coefficient on the K + O coadsorbate. The inhibitory effect of the K + O coadsorbate on hydrogen adsorption explains the existence of a reaction front. As a consequence of this inhibition effect, oxygen is presumably predominantly removed by diffusing hydrogen from the front region and not by hydrogen adsorbing directly from the gas phase.

The data in Figure 13 at first sight seem to indicate that the reactivity of the HCCP phase is higher, because the HCCP components disappear upon H_2 titration whereas the O_{tr} component remains as demonstrated by spectra 2 and 3 in Figure 13a. A higher reactivity of the HCCP would, however, be at variance with the results reported in ref 13. The previous conclusion would only be correct, however, if no oxygen were redistributed between the two states. If such a redistribution takes place, it is the total oxygen coverage that controls which phase

is present. In fact, a close inspection of the O 1s spectra in Figure 13a clearly shows that the disappearance of the HCCP component is accompanied with reduction of the total oxygen coverage to a level where the HCCP state is no longer stable.

The above experiment demonstrates that a potassium redistribution via fronts is also occurring in titration experiments without the supply of both gases. For the formation of the HCCP, three conditions apparently have to be fulfilled: (i) oxygen supply from the gas phase, (ii) a high enough K coverage, and (iii) a temperature above 570 K.

4. Discussion

4.1. Formation of the Condensed Phase. As demonstrated by successful simulations with a realistic mathematical model, the basic mechanistic features of the reaction-induced redistribution of potassium on Rh(110) can be considered as being well understood.[14] The key for understanding such a complex system relies on the complementary information provided by three spatially resolving in situ methods: PEEM, which images the local work function and yields the spatiotemporal dynamics; SPEM, which is a spectromicroscopic technique, providing chemical information; and LEEM, which is mainly based on diffraction contrast and thus is sensitive to structural changes. The LEEM and PEEM results have been reported in earlier publications.[7,9,27] Here, we discuss the SPEM profiles which yield chemical information and can be interpreted directly.

The above experiments on front propagation clearly show that the $O_2 + H_2$ reaction is no longer bistable in the presence of coadsorbed potassium. Nevertheless, the system still bears some features reminiscent of bistability. At least at higher temperature ($T > 570$ K), the direction of front motion can be reversed by a parameter change. The enrichment of potassium in the front region has been shown to be a kinetic effect. Simulations have shown that the different K diffusivity on the reduced and oxygen-covered surface suffices to explain this effect.[7]

A consequence of the reaction fronts being transients in the formation of a stationary pattern is that the front profiles depend on the history of the experiment, i.e., on the time schedule according to which the experimental p, T parameters are varied. Our experiments nevertheless are quite reproducible, so that probably only minor details of the front profiles are affected.

As shown by the energy diagram in Figure 3, a thermodynamic driving force exists for the condensation of K + O into large islands. In addition, kinetic feedback mechanisms also exist, stabilizing the coadsorbate phase. A positive feedback for the accumulation of a high oxygen coverage exists because the condensation of potassium promotes the dissociative adsorption of oxygen, leading to a higher local oxygen, which, in turn, favors K condensation. The K + O islands formed are also stabilized by their reduced reactivity toward hydrogen. The lowering of the reactivity of oxygen in the coadsorbed state was demonstrated in H_2 titration experiments using fast XPS to monitor the oxygen coverage.[13] As discussed in ref 13, the reduced rate of H_2O formation within the condensed islands can be attributed to site blocking for dissociative H_2 adsorption.

A particular role is evidently played by the (8×2) K + O coadsorbate structure found in the core of the condensed phase at $T > 570$ K. Because of its high K and O coverage, this structure has been termed the high-coverage condensed phase (HCCP). Unlike the other phases of the coadsorbate system Rh(110)/K + O the HCCP exhibits a shift in the Rh 3d core level similar to that of a surface "oxide". The same shift in Rh 3d has been observed in the incommensurate (8×8) O layer on Rh(111).[19] The reactivity is still too large for a true oxide phase, and therefore, the alternative explanation for a shift in the Rh 3d level of several oxygen atoms being coordinated to the same Rh atom appears to be more appropriate. The redistribution of oxygen between the HCCP and the O_{tr} phase in the titration experiments (Figure 13) also shows that this structure is not very rigid but easily transforms depending on the reaction conditions. One can therefore call it a surface oxide. The formation of such an oxide-like phase is evidently catalyzed by potassium similarly to alkali metal on other noble metals catalyzing the development of oxides. The fact that this structure appears in the core of the condensed phase can tentatively be attributed to a high thermodynamic and kinetic stability, with the latter term simply referring to its reduced reactivity against hydrogen. A previous investigation has demonstrated that the reactivity of the K + O structures decreases strongly with increasing K concentration.[13] The data in Figures 12 and 13 show this directly.

One consequence of coadsorbed potassium reducing the reactivity of oxygen is that the alkali metal actually acts as a poison and not as a promoter for the $O_2 + H_2$ reaction on Rh(110), thus lowering the rate of H_2O production. If we compare the poisoning effect of alkali metal being homogeneously distributed over the surface or being condensed into large islands, then the poisoning effect should be minimized through the condensation process. A small part of the surface would be deactivated, but the main part, being free of the alkali metal, would retain its high activity.

A μ-LEED/LEEM study of the condensation process at 573 K revealed that, in the long K tail extending far into the still oxygen-covered area, a (1×2) pattern is dominant, superimposed with weak satellite spots indicating an 8−12-fold periodicity in the [110] direction.[9] This means that, in the K + O coadsorbate region prior to the formation of the actual condensed phase, a phase separation must have taken place into a K-dense phase, the HCCP, and a K-dilute phase characterized by a (1×2) reconstruction of the substrate.

This microscopic phase separation is consistent with the XPS results of Figure 13, which also indicate that the HCCP is present prior to condensation. Evidently, this microscopic phase separation is tied to certain reaction conditions because, at 623 K (Figure 11), the HCCP develops only in the final stage of the condensation process. Because the HCCP does not form below 570 K, a temperature interval between 570 and 623 K apparently exists in which this microscopic phase separation occurs. The phase separation modifies the picture for K diffusion on the oxygen-covered surface, because the macroscopic gradient of the K concentration now translates microscopically into a gradient in the density of the HCCP islands.

4.2. Classification of the Stationary Patterns. Stationary concentration patterns (Turing structures) can develop in a reacting medium when a fast-diffusing inhibitor is present together with a slow-diffusing activator.[18,23] Although stationary concentration patterns (Turing structures) in chemical reaction systems were predicted more than 5 decades ago, surprisingly few experimental realizations have been achieved to date.[24] For liquid-phase reactions, the difficulties in obtaining a Turing structure are quite evident because the basic requirement of having reacting species with strongly varying diffusion coefficients is not met. In the liquid phase, all (small) molecules diffuse about equally fast. On catalytic surfaces, where the mobility of surface species can vary enormously, the chances for the formation of Turing structures appear quite favorable,

but with the exception of the reaction-induced roughening of a Pt(110) surface, no experimental example has been presented so far.[25]

The irregularly shaped condensation islands formed by reduction fronts in our system seemed to be quite in contradiction to the basic requirement for a Turing structure of a periodic pattern developing from a spatially homogeneous state. As it was suspected that these differences might not be due to the true properties of the system but might just reflect the too-slow mobility of potassium on the oxygen-covered surface, the experimental procedure was modified. Instead of starting from an oxygen-covered surface as in the preceding experiments, the experiment was started from reducing conditions. In fact, a periodic concentration pattern developed from the homogeneous state thus seemingly fulfilling the criteria for a Turing structure.[26] These periodic patterns were also reproduced in simulations.[14] The patterns are nevertheless different from a "classic" Turing structure, because in a classic Turing structure, only the different diffusion rates of the reacting species are responsible for an instability whereas, in our case, energetic interactions between adparticles and non-Fickian diffusion are essential. The length scale of the islands is mainly determined by potassium diffusion, as shown in realistic simulations.[7,14]

A phase separation caused by attractive interactions can occur even in the absence of reaction, and a very simple example is any system exhibiting a first-order phase transition such as a van der Waals gas. In our case, it is clear that both the reaction and the attractive interactions are essential for producing the condensed islands. The patterns discussed can be termed Turing-like, but in light of the previous arguments, this classification is imprecise and a more appropriate description would be reactive phase separation.

4.3. Other Systems and Implications for Catalysis. From the mechanism sketched above, the requirements to observe similar condensation processes in other systems as well appear to be quite loose: an alkali metal (AM) together with a catalytic reaction involving some electronegative species with which the AM can react seem to suffice. With spatially resolved methods, so far only the systems Rh(110)/Cs/O_2 + H_2,[27] Rh(110)/Cs + K/O_2 + H_2,[27] Rh(110)/K/NO + H_2,[28] and Rh(110)/Pt/K/O_2 + H_2,[29] as part of an investigation of microstructured surfaces, have been studied. In the system Rh(110)/Cs + K/O_2 + H_2, in addition to the well-known condensation process, surprisingly, a macroscopic phase separation of the two alkali metals was also observed. The intensely studied NO + H_2 reaction on Rh(110) is an excitable system exhibiting travelling pulses on the background of an oxygen-covered surface. With coadsorbed potassium, the potassium binds to the oxygen but not to the nitrogen so that the travelling pulses are transporting potassium.[28] Finally, the condensation patterns which were seen on the Pt domains of a microstructured Rh(100)/Pt surface during the O_2 + H_2 reaction provided the original motivation for studying the behavior of alkali metals on catalytic surfaces.[30] These stationary patterns had originally been interpreted as being a property of the system Rh(110)/Pt/O_2 + H_2, and only when the presence of potassium as a contaminant was discovered did it become clear that the influence of the alkali metal should be investigated more closely. It became evident that alkali condensation under reaction conditions was the primary pattern-forming process on the microstructured Rh(110)/Pt surface.[29,31]

In heterogeneous catalysis, a significant number of technologically important reactions employ alkali metals as so-called electronic promoters. The promoter effect is explained in terms of a local modification of the electronic surface of a transition metal.[1,5] If, aside from the local modification, some large-scale structures of the AM were also present under reaction conditions, the overall picture of how a promoter works in real catalysis would clearly be different. One can expect that condensation processes similar to the one studied here will occur in catalytic reactions that involve some electronegative species, including, for example, Fischer−Tropsch synthesis. To show that this is actually the case, spatially resolved in situ studies at high pressure would be required.

The conditions under which a reactive phase separation of the type described here should occur are, in fact, not at all restrictive. One should expect similar effects in systems with mobile promoters and poisons and, furthermore, in all bimetallic systems in which one constituent is mobile and exhibits a high affinity to one of the reacting species.

5. Conclusions

Using calibrated K concentration profiles, the reversible condensation process of potassium in the system Rh(110)/K/O_2 + H_2 has been studied quantitatively. Front propagation can be reversed by a parameter change at $T > 570$ K. The enrichment of potassium in the front region was shown to be caused by the low mobility of potassium on the oxygen-covered surface and not by a different chemical environment in the front region. At low temperature, i.e., $T \leq 550$ K, probably again limited by the low mobility of potassium on the oxygen-covered surface, potassium is only partially redistributed by reduction fronts, and a substantial amount of K + O coadsorbate remains on the reduced surface. At high temperature, i.e., $T = 623$ K, nearly complete redistribution is achieved. In the core of the condensed phase, one finds a (8×2) K + O coadsorbate structure characterized by a shift in the Rh 3d peak and an additional O 1s state at 528.8 eV. Critical conditions for the formation of this oxide-like structure during the catalytic reaction are a temperature above 570 K, a potassium coverage of at least $\Theta_K = 0.19$, and a continuous supply of oxygen from the gas phase.

References and Notes

(1) Bonzel, H. P., Bradshaw, A. M., Ertl, G., Eds. *Physics and Chemistry of Alkali Metal Adsorption*; Elsevier: Amsterdam, 1989.
(2) Kiskinova, M. *Poisoning and Promotion in Catalysis Based on Surface Science Concepts*; Elsevier: Amsterdam, 1992.
(3) Diehl, R. D.; McGrath, R. *Surf. Sci. Rep.* **1996**, *23*, 43.
(4) Over, H. *Prog. Surf. Sci.* **1998**, *58*, 249.
(5) Mortensen, J. J.; Hammer, B.; Norskov, J. K. *Surf. Sci.* **1998**, *414*, 315.
(6) Marbach, H.; Günther, S.; Luerssen, B.; Gregoratti, L.; Kiskinova, M.; Imbihl, R. *Catal. Lett.* **2002**, *83*, 161−164.
(7) Marbach, H.; Hinz, M.; Günther, S.; Gregoratti, L.; Kishkinova, M.; Imbihl, R. *Chem. Phys. Lett.* **2002**, *364*, 207.
(8) Günther, S.; Marbach, H.; Lurssen, B.; Imbihl, R.; Gregoratti, L.; Barinov, A.; Kiskinova, M. *Surf. Rev. Lett.* **2002**, *9*, 751.
(9) Marbach, H.; Lilienkamp, G.; Wei, H.; Günther, S.; Suchorski, Y.; Imbihl, R. *PCCP* **2003**, *5*, 2730.
(10) Esch, F., manuscript in preparation.
(11) Kiskinova, M.; *Chem. Rev.* **1996**, *96*, 1431.
(12) Comelli, G.; Dhanak, V. R.; Kiskinova, M.; Prince, K. C.; Rosei, R. *Surf. Sci. Rep.* **1998**, *32*, 165.
(13) Günther, S.; Marbach, H.; Hoyer, R.; Imbihl, R.; Baraldi, A.; Lizzit, S.; Kiskinova, M. *J. Chem. Phys.* **2003**, 119.
(14) Hinz, M.; Günther, S.; Marbach, H.; Imbihl, R. *J. Phys. Chem. B*, in press, 2004. Hinz, M. Doctoral Thesis, Universität Hannover, Hannover, Germany, 2003.
(15) Kiskinova, M.; Fabrizio, E. D.; Gentili, M.; Marsi, M. *Surf. Rev. Lett.* **1999**, *6*, 265.
(16) Mertens, F.; Imbihl, R. *Chem. Phys. Lett.* **1995**, *242*, 221.
(17) Makeev, A.; Imbihl, R. *J. Chem. Phys.* **2000**, *113*, 3854.
(18) Mikhailov, A. S. *Foundations of Synergetics*; Springer: Berlin, 1991.

(19) Gustafson, J.; Borg, M.; Mikkelsen, A.; Lundgren, E.; Andersen, J. N. *Max-Lab Annual Report*; 2001; p 144.

(20) Ganduglia-Pirovano, M. V.; Scheffler, M.; A. B.; Lizzit, S.; Comelli, G.; Paolucci, G.; Rosei, R. *Phys. Rev. B* **2001**, *63*, 205415.

(21) Vesselli, E.; Africh, C.; Baraldi, A.; Comelli, G.; Esch, F.; Rosei, R. *J. Chem. Phys.* **2001**, *114*, 4221.

(22) Baraldi, A. Private communication.

(23) Kapral, R., Showalter, K., Eds. *Chemical Waves and Patterns*; Kluwer: Dordrecht, The Netherlands, 1994.

(24) Turing, A. M. *Philos. Trans. R. Soc.* **1952**, *B237*, 37.

(25) Imbihl, R.; Reynolds, A. E.; Kaletta, D. *Phys. Rev. Lett.* **1991**, *67*, 275.

(26) De Decker, Y.; Marbach, H.; Hinz, M.; Günther, S.; Kiskinova, M.; Mikhailov, A. S.; Imbihl, R.; Phys. Rev. Lett. **92**, 198305 2004.

(27) Marbach, H. Doctoral Thesis, Universität Hannover, Hannover, Germany, 2002.

(28) Marbach, H.; Günther, S.; Neubrand, T.; Imbihl, R. *Chem. Phys. Lett.*, in press.

(29) Günther, S.; Marbach, H.; Hoyer, R.; Imbihl, R.; Gregoratti, L.; Barinov, A.; Kiskinova, M. *J. Chem. Phys.* **2002**, *117*, 2923.

(30) Schütz, E.; Esch, F.; Günther, S.; Schaak, A.; Marsi, M.; Kiskinova, M.; Imbihl, R. *Catal. Lett.* **1999**, *63*, 13.

(31) Imbihl, R. *Chaos* **2002**, *12*, 182.